




# Electrodeposition of Bi<sub>2</sub>Te<sub>3</sub> thin films for thermoelectric applications: effect of electrolyte pH

Vinod S. Khairnar<sup>1,\*</sup> , Anil N. Kulkarni<sup>2</sup>, Vishal V. Lonikar<sup>3</sup>, Anil B. Gite<sup>4</sup>, Mirtunjay Kumar<sup>5</sup>, Dipak P. Patil<sup>6</sup>, and Deepak P. Kadam<sup>1</sup>

<sup>1</sup>Department of Engineering Sciences, METs Institute of Engineering, MET Bhujbal Knowledge City, Nashik, India

<sup>2</sup>Department of Physics, NTVS's Patil Arts, Science and Commerce College, Nandurbar, India

<sup>3</sup>Department of Physics, Bhujbal Academy of Science and commerce, MET Bhujbal Knowledge City, Nashik, India

<sup>4</sup>Department of Physics, SNJB's Arts and Science College, Nashik, India

<sup>5</sup>Department of Materials, University of Manchester, Manchester, UK

<sup>6</sup>Department of Electronics and Telecommunication, Sandip Institute of Engineering and Management, Nashik, India

Received: 9 January 2023

Accepted: 19 March 2023

Published online:

3 April 2023

© The Author(s), under exclusive licence to Springer Science+Business Media, LLC, part of Springer Nature 2023

## ABSTRACT

Modern materials like Bi<sub>2</sub>Te<sub>3</sub> nanostructures are one of the most promising thermoelectric materials since they show a high value of the thermoelectric figure of merit. This paper reports the effect of electrolyte pH (in a low pH range starting from 0.25 to 1.50) on the structural, electrochemical, and thermoelectric properties of the electrodeposited Bi<sub>2</sub>Te<sub>3</sub> films. Two of the samples showed significantly high values of Seebeck coefficient (49.28 μV/T and 45.26 μV/T, respectively), which are comparable to the Si (42 μV/T), SiC nanowires (40 μV/T), and Ge (47 μV/T) thermoelectric materials. Also, the observed crystallinity and electrochemical behavior are in agreement with the thermoelectric results for electrodeposited Bi<sub>2</sub>Te<sub>3</sub> films. In nutshell, a lower range of pH of electrolytes has been found to be a significant control parameter in the present study. Such Plausible tailoring of properties would be helpful for the systematic study of complex and multi-composite materials for various applications.

## 1 Introduction

There are many thermoelectric materials being studied in the form of thin films. Materials like Bismuth Chalcogenides [1], Lead tellurides [2, 3], Inorganic Clathrates [4, 5], Mg-B<sup>IV</sup> compounds [6, 7], Homologous oxides [8, 9], Half-Heusler alloys [10, 11] etc.

Among these materials, in the current thread of research, Bi<sub>2</sub>Te<sub>3</sub> has been studied extensively. This is

due to its high value of thermoelectric figure of merit at room temperature. In addition, out of many methods of synthesis, electrodeposition method has been explored by the researchers. Electrodeposited Bi<sub>2</sub>Te<sub>3</sub> nanowire arrays (12–33 μV/K), pulse electrodeposited Bi<sub>2</sub>Te<sub>3</sub> thin films (– 65 μV/K), and *n*-type Bi<sub>2</sub>Te<sub>3</sub> films (– 51.6 μV/K) had shown Seebeck coefficient ranging from 12 to 65 μV/K [12–14].

Address correspondence to E-mail: vinodk\_ioe@bkc.met.edu

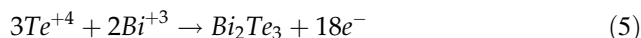
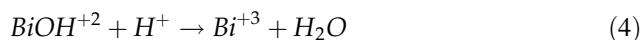
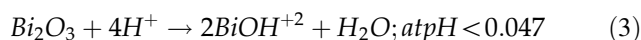
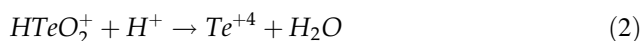
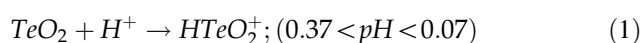
Electrodeposited thin films exhibit excellent thermoelectric properties as a function of reaction parameters [15–21]. In addition, the deposition rate of various phases followed by crystallite sizes can be controlled via electrodeposition parameters. And hence, this method is suitable for depositing thin films for the purpose of thermoelectric applications.

Theoretically, a material has better thermoelectric properties if electrical conductivity of the material is high and thermal conductivity of the material is low. A conductor or a semiconductor material shows thermal conductivity on account of two major phenomena viz. transport of heat through charge carriers and transport of kinetic energy through particle like behavior of lattice vibrations known as phonons. Transport of charge carriers contributes to both thermal and electrical conductivity. Thus, higher electrical conductivity by virtue of charge carrier transport also increases the thermal conductivity by this route. However, the amount of heat transported through phonons is decided by the crystal structure and crystallite size in case of crystalline solids [22, 23]. Thus, for a thermoelectric material, we need to optimize the crystallite size for optimal electric and thermal conductivities. Many studies have been reported for the deposition of  $\text{Bi}_2\text{Te}_3$  films. However, the tailoring of the structural, electrochemical, and thermoelectric properties as a function of lower range of pH has not been explored in detail. Thus, it is indeed necessary to investigate such dependence of different properties over a reaction parameter(s). And, it may be helpful, since nowadays even more complex and multi-composite materials (like perovskite) are being studied not only for thermoelectric but also for other properties like semiconducting, photoelectric, and supercapacitive actions.

The purpose of setting the parameters is to achieve thermodynamically optimal conditions for electrochemical deposition of ions on to the substrate as well as nucleation and growth of material in the electrolyte. For this purpose, under potential deposition method was used to ensure a uniform and thin deposition of the material. The stainless-steel plates were chosen to be the deposition substrate. According to literature review, mutually induced co-deposition of  $\text{Bi}^{3+}$  and  $\text{Te}^{2+}$  ions happens if correct electrochemical parameters are set [15, 18]. The ions will be deposited together at a potential more positive than both the deposition potentials of individual ions. It is also required that formation of the said ions

must occur when the precursors are dissolved into the solvent. With these conditions in place, optimized deposition potential was explored earlier and found out to be  $-400$  mV/SCE at room temperature [20]. To optimize thermal and electrical properties as function of crystallinity through exploring the lower range of pH for electrodeposition of  $\text{Bi}_2\text{Te}_3$  thin film is the aim of present study.

In this article, we report the properties of 6 films that were deposited at the optimum deposition potential of  $-400$  mV/SCE with pH varying from 0.25 to 1.5 in the interval of 0.25 and designated as P1 to P6, respectively. The range for pH parameter is selected as per the Pourbaix diagram for electrodeposition carried out with the route as stated below [15]



For Eqs. 1–4, the rate of the reaction will be decided by the  $\text{H}^+$  ion concentration, i.e., pH of the solution. Since pH of the electrolytes decides the deposition rates of Bi and Te, the quality of co-deposited product is in turn impacted. Quality parameters include purity (relative amounts of  $\text{Bi}_2\text{Te}_3$ , Te, Bi, and other compounds) and crystallinity (phases and crystallite size). These parameters affect the electrical and thermal properties of the deposited material which is to be used for thermoelectric applications.

## 2 Experimental procedures

In the present synthesis, solutions of A.R. grade bismuth nitrate ( $\text{Bi}_2(\text{NO}_3)_3 \cdot 5\text{H}_2\text{O}$ ) and tellurium dioxide ( $\text{TeO}_2$ ) were prepared in nitric acid ( $\text{HNO}_3$ ), respectively, in two different beakers, wherein  $\text{Bi}_2(\text{NO}_3)_3 \cdot 5\text{H}_2\text{O}$  acts as a precursor of  $\text{Bi}^{3+}$  and  $\text{TeO}_2$ , that of  $\text{Te}^{2+}$  explained in the following steps as shown in Fig. 1 [15, 18, 20].

First, the bath of 7.5 mM  $\text{Bi}^{3+}$  was prepared by adding 0.90 gm of bismuth nitrate in 250 ml of 1 M nitric acid and kept for 15 min until a uniform mixture was formed. Second, 0.1 M ethylene diamine

tetra acetic acid (EDTA), a complexing agent, was then prepared in 100 ml double distilled water. Third, 3 ml of 0.1 M EDTA then added to the first bath containing bismuth source to obtain  $\text{Bi}^{3+}$  EDTA complex. Fourth, 10 mM solution was prepared in 1 M (250 ml) of nitric acid under constant stirring at 80 °C temperature for 30 min. Fifth, 13.5 ml of  $\text{Te}^{2-}$  precursor solution was slowly introduced into the 16.5 ml that of  $\text{Bi}^{3+}$  EDTA complex precursor solution under constant stirring. The pH of prepared electrolyte was varied from 0.25 to 1.5 with increase of 0.25 using liquor ammonia. The reaction is considered to be based on slow release of  $\text{Bi}^{3+}$  and  $\text{Te}^{2+}$  ions in the presence of EDTA, which helps for obtaining the soluble species of the  $\text{Bi}^{3+}$  in acidic medium during the synthesis process [4]. The electrodeposition was carried out for different pH [P1–P6] of electrolyte mixture of 7.5 mM  $\text{Bi}^{3+}$  and 10 mM  $\text{TeO}_2$  at  $-400$  mV/SCE at room temperature for the deposition time of 40 min and named as P1–P6, respectively. The flowchart in Fig. 1 shows the stepwise process involved in the electrodeposition of  $\text{Bi}_2\text{Te}_3$  thin films as function of pH [15, 18, 20].

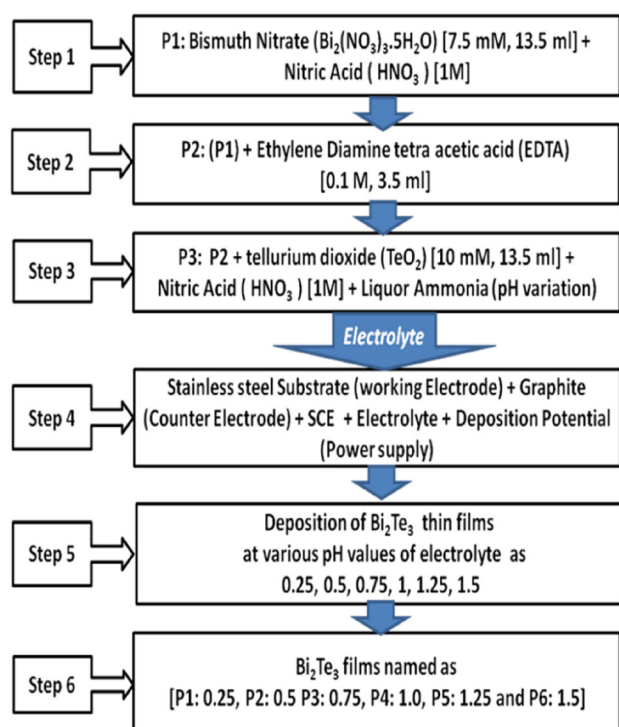


**Fig. 1** Stepwise process involved in the electrodeposition of  $\text{Bi}_2\text{Te}_3$  thin film of samples (P1–P6)

### 3 Results and discussion

The prepared films were characterized to determine the properties viz. elemental composition, crystal structure, phase, crystallite size, morphology, thickness, and thermoelectric properties (Seebeck Coefficient, Power Factor and Figure of merit). These results are presented and discussed below.

Cyclic voltammetry (CV) analysis for precursors and their mixture at various pH and concentration was carried out using Potentiostat Interface model 1000 (IFC100004015, Garmry). Thicknesses of the all the deposited films were measured with weighing balance made by Shimadzu (AUX220) having least count of 10 mg. Structural analysis and phase detection of the  $\text{Bi}_2\text{Te}_3$  crystals in the electrodeposited films were carried out with the help of Panalytical Xpert PRO X-ray diffractometer (XRD) with  $\text{Cu K}\alpha$  radiation ( $\lambda = 1.5405$  Å). Surface morphology and compositional analysis were carried out using a scanning electron microscope (JEOL-JSM 6360) (SEM) with energy-dispersive X-ray spectroscopy (EDXS) Hitachi High (S 4800 Type II) with acceleration voltage at 20 kV. Electronic properties were studied using Hall probe method ECOPIA hall effect measurement system (HMS-3000). Seebeck coefficient measurement was carried out with the laboratory made setup (Two K type thermocouples, Rishabh multimeter (Multi 14S), HTC (DT302) Thermometer). Thermal conductivity was measured with the Nano-flash (LFA 447) Netzsch instrument. The phase analysis of samples using XRD patterns has been made using Xpert Highscore package with Reference Intensity Ratio (RIR) method (more confident).

#### 3.1 Cyclic voltammetry

Cyclic voltammetry curves were recorded during deposition process and are shown in Fig. 2 for the films P1–P6 (7.5 mM  $\text{Bi}^{3+}$ , 10 mM  $\text{TeO}_2^{2+}$ , and 0.1 M EDTA). The curves show distinct oxidation and reduction peaks within the potential range of  $-400$  mV/SCE to 700 mV/SCE. For P1 film, we see an oxidation peak at 432.0 mV and reduction peaks at  $-343.9$  mV and  $-250$  mV. The reduction peaks indicate the deposition of Te ions through two different modes [15]. Single oxidation peak for P1, P2, and P3 CV curves indicates that deposited material indeed is  $\text{Bi}_2\text{Te}_3$ . However, in case of P1 and P2, the presence of Nucleation loop indicates irreversible Te–

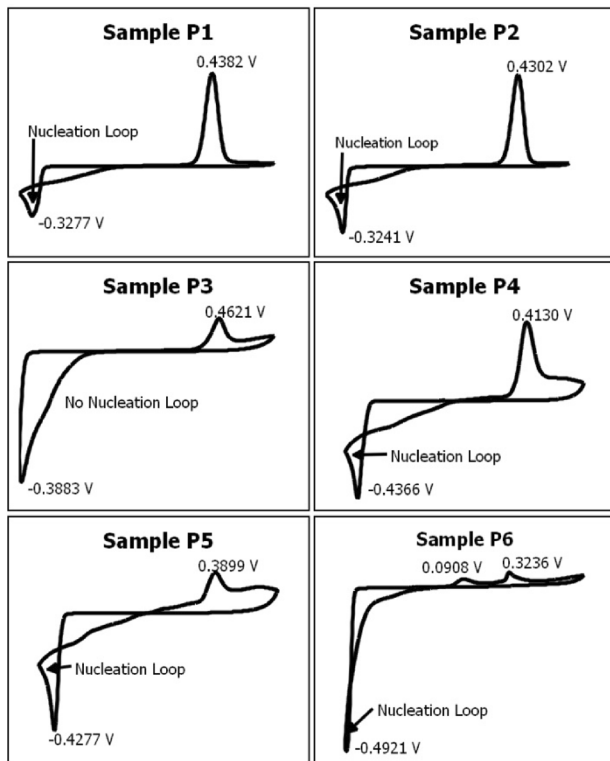


**Fig. 2** Cyclic voltammograms  $\text{Bi}_2\text{Te}_3$  with different pH values from (P1–P6)

Te deposition [15], while in case of P3, large reduction peak indicates dominant but reversible Te–Te deposition. While in case of P4, P5, and P6 films, there is additional small oxidation peak after the Bi oxidation peak. This may correspond to decomposition of Te or Bi atoms. In case of P4 and P5, the nucleation loop similar to that in P1 and P2 indicates irreversible Te–Te deposition. In addition to the major reduction and oxidation peaks, there are other oxidation and reduction peaks present in case of Samples P4 and P5 which again may correspond to decomposition of the deposited Bi and Te.

Another major aspect of the CV analysis is regarding movement of the oxidation and reduction peaks with the pH parameter. P2 shows dominant deposition of Bi at moderate oxidation potential of 4.302 V while P1, P3, and P4 show such deposition at higher potential and P5 and P6 at lower potential.

In case of deposition of Te by reduction, P2 shows lowest negative potential of (– 0.3241) for deposition while all other samples show reduction peaks of Te at a larger negative potential [12].

### 3.2 Thickness

Thicknesses of the films were measured using indirect weighing difference method. The average thicknesses of the films are plotted in Fig. 3. P2 sample shows the largest average thickness while P4 shows the smallest. This parameter indicates the rate of deposition of the material since the films are deposited within the same amount of time interval. Thickness of the material was assumed to be uniform as we are using electrochemical method for deposition.

Any parameter that is calculated here onward is intrinsic parameter. It is desirable to have thinner films so that the parameters will be better since the parameters are usually calculated per unit volume or mass.

### 3.3 X-ray diffraction

X-ray diffraction patterns for all the samples are shown in Fig. 4. The XRD patterns show the presence of polycrystalline structure. Signature peaks of  $\text{Bi}_2\text{Te}_3$  around  $2\theta \sim 27.74^\circ$ ,  $41.02^\circ$ ,  $44.32^\circ$ , and  $50.44^\circ$  corresponding to (h k l) planes (0 1 5), (1 1 0), (0 0 15), and (2 0 5) [24], respectively, are seen in all the samples. Intensities of the most prominent peak (0 1 5) can be seen to have different intensities relative to other peaks for different samples.

Further, Table 1 shows the average crystallite sizes, micro-strains, and dislocation densities for the films P1 to P6 obtained using the full width at half-maximum (FWHM) from XRD patterns.

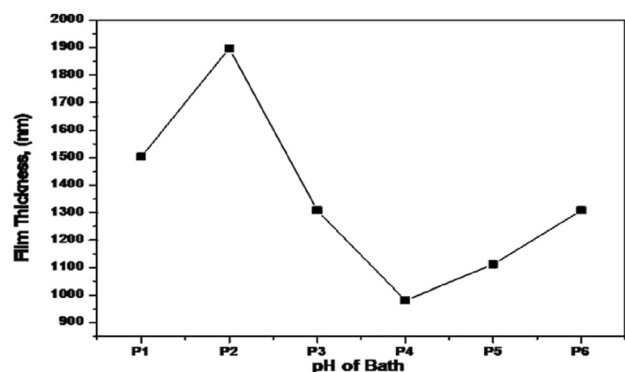


**Fig. 3** Thickness variation of the samples (P1–P6) for deposition time of 40 min

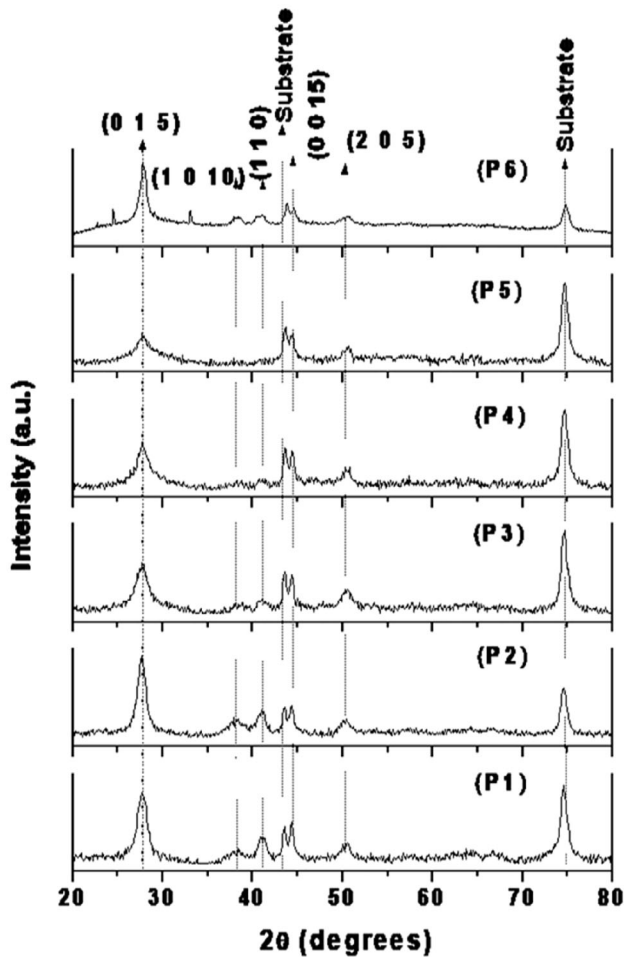


Fig. 4 X-ray diffraction patterns of samples (P1–P6)

Table 1 XRD analysis for [0 1 5] plane

#	2θ	a	β	D	ε	δ
P1	27.74	3.21	1.122	7.61	47.53	231.77
P2	27.54	3.23	1.108	7.71	46.61	171.82
P3	27.68	3.22	1.124	6.89	52.53	261.17
P4	27.72	3.21	1.565	5.46	66.30	415.94
P5	27.72	3.21	1.702	5.02	72.10	491.95
P6	27.81	3.20	0.871	9.81	36.84	128.78

# sample number, 2θ Bragg’s Angle in degrees, a lattice parameter in angstroms, β FWHM in degrees, D crystallite size in nanometres, ε microstrain in 10<sup>16</sup> linesm<sup>-2</sup> and δ dislocation density in 10<sup>-4</sup>line<sup>-2</sup> m<sup>-4</sup>

For the analysis, Scherer’s equation and standard JCPDS card No: 15-0863 [24] for Bi<sub>2</sub>Te<sub>3</sub> were used. Scherer’s equation is given below:

$$\tau = \frac{K\lambda}{\beta\cos(\theta)}$$

where, τ is the mean crystalline domains size, K is the shape factor, λ is the X-ray wavelength, β is the FWHM, and θ is the Bragg angle.

Samples P1, P2, and P6 show narrower and larger (0 1 5) peak while P3, P4, and P5 show wider and smaller (0 1 5) peaks. Widening of the peaks is due to small crystallite size (in nanometres) as well as due to induced microstrain in the films. Larger intensities of the material compared to peaks of the substrate indicate larger phase percentage. (1 0 10) and (1 1 0) peaks are present prominently in only P1, P2, and P3 samples. (0 0 15) peak is present in all the samples but for P6, the peak is smaller as compared to other samples. Note that the samples P2 and P6 show all the peaks and larger (0 1 5) peak as compared to the substrate peak. From this analysis, we conclude that P2 and P6 must have significant amount of Bi<sub>2</sub>Te<sub>3</sub> crystallites. This is further confirmed by phase analysis performed using RIR method from XRD data as indicated in Fig. 5.

The crystallite size analysis indicates that P6 followed by P2 has the largest crystallite size and thus the lowest microstrain.

### 3.4 Elemental analysis

Elemental analysis performed using EDAX is shown in Table 2. Samples P2, P3, and P4 are relatively closer to the actual stoichiometric ratio of 0.67 for the compound. However, it has been proved before that this material can exist in same phase with different

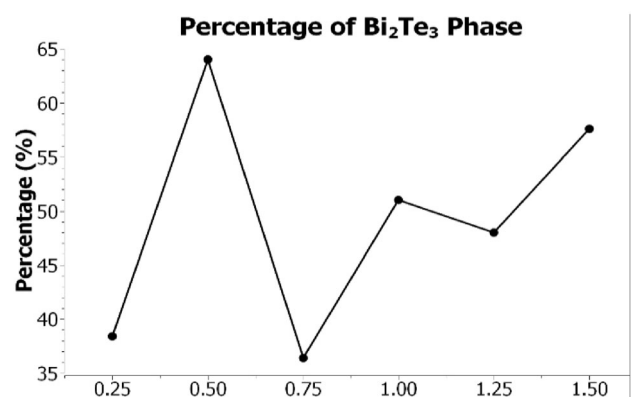


Fig. 5 Bi<sub>2</sub>Te<sub>3</sub> Phase amount for the samples (P1–P6) using XRD data

**Table 2** Elemental analysis for samples (P1–P6)

Sample	Bi%	Te%	Bi/Te
P1	54.28	45.72	1.19
P2	49.31	50.69	0.97
P3	46.43	53.57	0.87
P4	48.94	51.06	0.96
P5	57.11	42.84	1.33
P6	57.90	42.10	1.38

stoichiometric ratios [15]. Samples P1, P5, and P6 are quite Bi rich as compared to other 3.

### 3.5 Scanning electron microscopy

Figure 6 shows the SEM images morphology of the samples. All samples exhibit dendritic masses fused together to various degrees (refer to high resolution figures located at the insets of the SEM images). SEM images show a fused mass of dendrites for P1 sample, relatively separated dendritic masses in the form of aggregated balls for P2. While P3 shows morphology similar to P2 but for P2, the balls have more clear boundaries than P3. The SEM image for P3 also shows two different areas, light and dark, which may be interpreted as follows. Dark area refers to a flatter morphology with less dense mass, while light areas refer to balls shaped areas. P4 shows morphology with dendrites forming a continuous mass similar to P1 but with larger voids which are in the case of this particular snap is all oriented along same direction. P5 and P6 both again show aggregated balls type morphology. But P6 has the dendritic structures more separated than P5.

Morphology of the structure is an important parameter since thermal as well as electrical conductivities depend on the morphology. One can conclude that, more fused dendritic structures results in to the good thermal conductivity. Such large values of conductivity are detrimental to the thermoelectric effect as per the obtained figure of merit (ZT) in the present work [25–27]. Thus, we expect P2 and P6 to perform better as a thermoelectric material provided they show good electrical conductivity.

### 3.6 Thermal conductivity

Thermal conductivities of the samples were measured and are plotted in the Fig. 7.

High thermal conductivity of P3 brings down the performance of the film, while P2 has relatively high but still low enough thermal conductivity in addition to the co-deposition-favored crystal structure which is favorable for better thermoelectric performance. For all other samples, the thermal conductivity is very low. If the electrical conductivities of these samples are high enough the samples will perform better as thermoelectric materials [22, 23].

### 3.7 Four probe

The electrical conductivities of the samples shown in Fig. 8 are measured using four probe methods. Highest conductivity was shown by the P3 sample while others show significantly lower conductivities. P2 exhibits second best value for conductivity. However, as stated, earlier to large value of thermal conductivity may become detrimental for a thermoelectric material. We may expect P2 to be one of the best thermoelectric materials from all the samples since it shows the combination of favored co-deposition, moderate thermal conductivity, as well as moderate electric conductivity.

Low conductivity despite large crystallite size of samples P1, P5, and P6 may be due to the Bi richness which was discussed in elemental analysis section.

Which means though these samples show larger crystallites, the crystallites may be surrounded by Bi-rich phases. Hence, such deposition shows lower conductivity despite of larger crystallite size, whereas samples P2 and P3 show large conductivity despite smaller crystallite size. In short, not only the amount of crystal boundaries but also the ease of conduction of charge carriers across a boundary will also affect the electrical and thermal conductivity.

### 3.8 Seebeck coefficient and figure of merit

The Seebeck coefficients plotted in Fig. 9 for the samples are calculated using a laboratory made setup. The best Seebeck coefficient as shown in Fig. 9 was exhibited by P2 sample followed by P6, P1, and P3. As mentioned earlier, the reason for the best performance of P2 may be the combination of moderate electrical conductivity, low thermal conductivity, and co-deposition dominated phase. This agrees with the phase analysis discussed in XRD section.

Figure of merit is a performance indicator used to compare the performance of the materials. In this

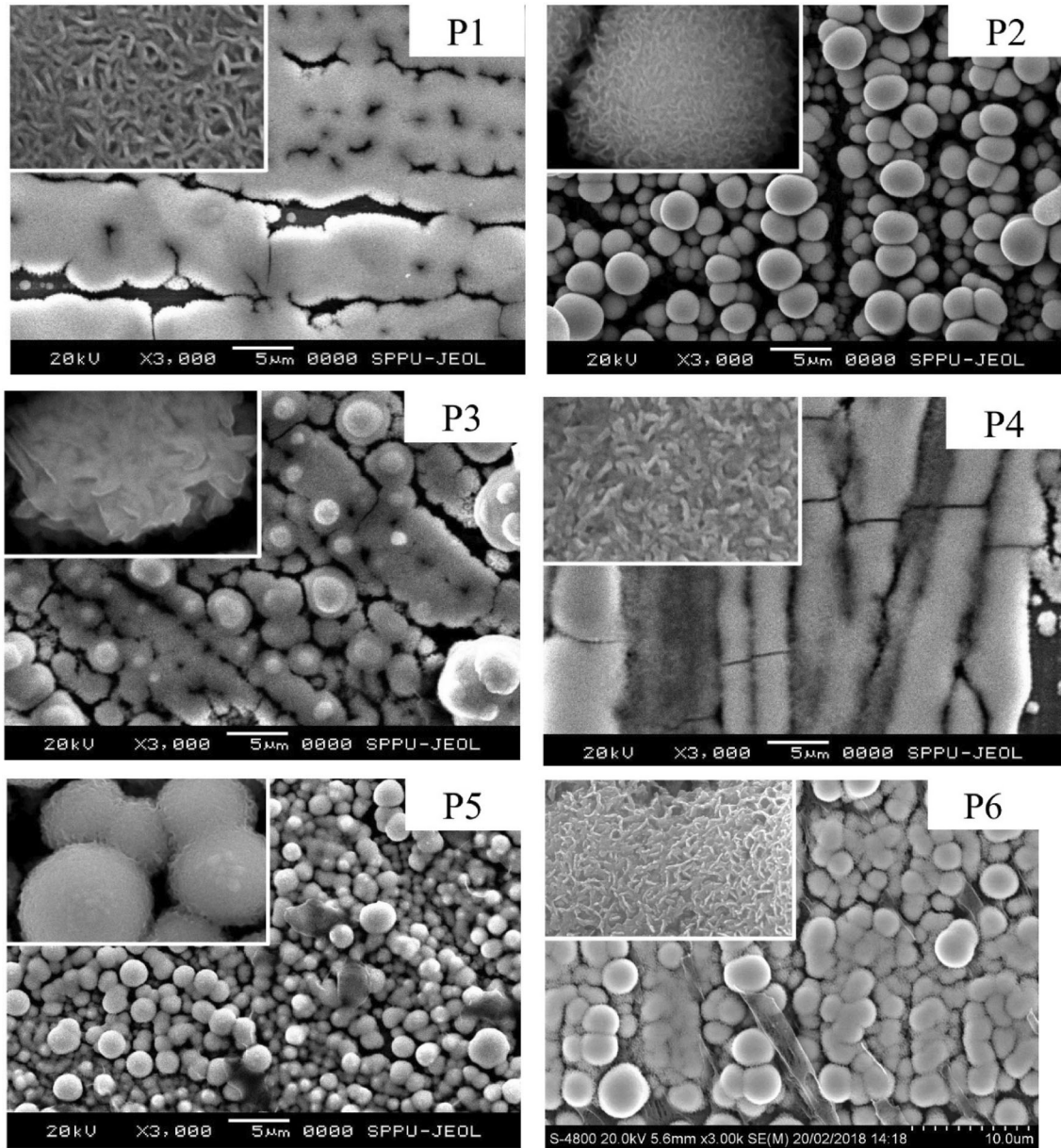


**Fig. 6** Scanning Electron Images of samples (P1–P6): 3000 × main images and 6000 × (higher resolution) images in inset

case, figure of merit to measure thermoelectric performance of a material is given by [25, 26, 28]

$$ZT = \frac{\sigma S^2}{\kappa} T$$

where  $\sigma$  is electrical conductivity,  $S$  is Seebeck coefficient,  $\kappa$  is the thermal conductivity, and  $T$  is the absolute temperature.

Hence, to achieve better thermoelectric properties, the material must have high electrical conductivity, Seebeck coefficient, and low thermal conductivity [15, 25, 28, 29].

Thermoelectric figure of merits for samples (P1–P6) are plotted in Fig. 10 and are calculated using the electrical conductivities, thermal conductivities, and Seebeck coefficient of the samples.

Taking into account all electrical conductivity (large for P3 and moderate for P2), Seebeck coefficient (large for P2 and moderate for P1, P3, and P6), and thermal conductivity (large for P3 and moderate for P3 while others have low thermal conductivities), P2 performs as the best thermoelectric material followed by P6, P3, P4–P5, and P1 as per the figure of merit (ZT).

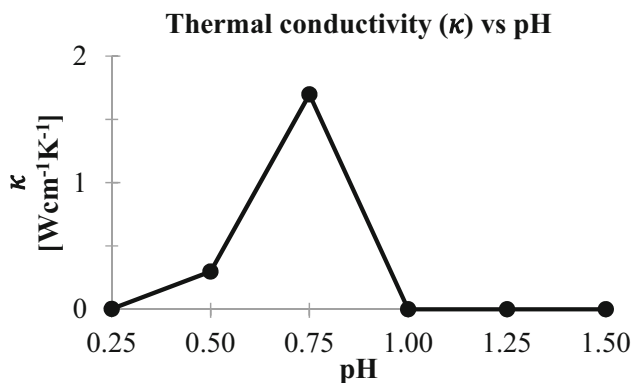


**Fig. 7** Variation of thermal conductivity with pH for samples (P1–P6)

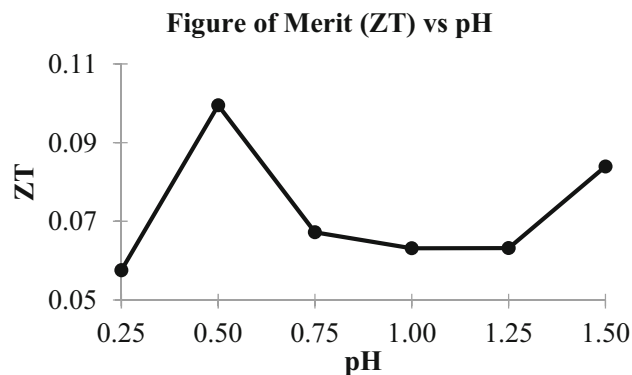


**Fig. 10** Variation of figure of merit with pH for samples (P1–P6)

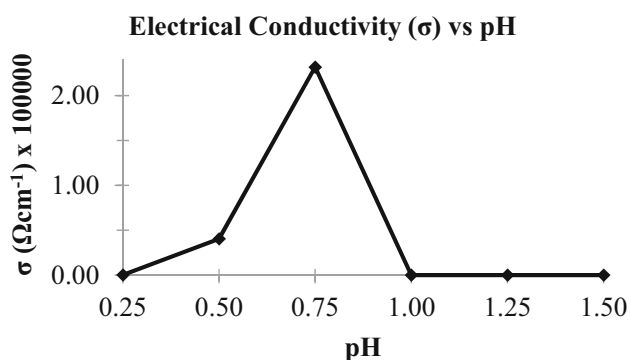


**Fig. 8** Variation of electrical conductivity with pH for samples (P1–P6)

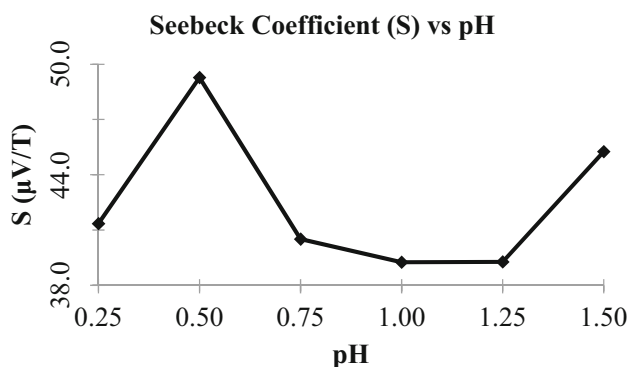


**Fig. 9** Variation of Seebeck coefficient with pH for samples (P1–P6)

## 4 Conclusion

The paper reports successful electrodeposition of  $\text{Bi}_2\text{Te}_3$  films for thermoelectric applications using lower pH as a control parameter. XRD and CV spectra revealed that pH has significant control over the rate of all redox reactions that are possible in

given electrolyte. Hence, pH in turn controls the rate of deposition of various phases of the substance on to the substrate. Thus, variation of the pH causes variation of thermal and electrical conductivities that in turn vary the thermoelectric properties of the deposited material. This is evident from the CV and structural results that complement the thermoelectric observations.

Sample P2 found to yield better  $\text{Bi}_2\text{Te}_3$  as a thermoelectric material ( $S = 49.28 \mu\text{V}/\text{T}$ ,  $ZT = 0.099$ ) than the Si ( $\sim 42 \mu\text{V}/\text{T}$ ) and Ge ( $\sim 47 \mu\text{V}/\text{T}$ ) thermoelectric materials. This performance is exhibited on account of moderate electrical conductivity and low thermal conductivity due to optimal crystallite size and phase amount. This suggests that optimization of other reaction parameters in combination with pH would open an interesting way out to study complex or multi-composite materials for various applications.

## Acknowledgements

This research did not receive any specific grant from any funding agencies in the public, commercial, or not-for-profit sectors. VSK is thankful to the Department of Engineering Physics, MET's Institute of Engineering, Nasik, for support and encouragement. VSK is grateful to Dr. V. P. Wani, Principal, MET's Institute of Engineering, Nashik. ANK is grateful to Management and Principal, NTVS's G T Patil Arts, Science and Commerce College, Nandurbar. VVL is thankful to the Management MET Bhujbal Knowledge City.



## Author contributions

All authors contributed to the study conception and design. Material preparation, data collection, and analysis were performed by VSK and ANK. Phase amount analysis from XRD was performed by MK<sup>5</sup>. The first draft of the manuscript was written by VVL and all authors commented on the previous versions of the manuscript. All authors read and approved the final manuscript.

## Funding

The authors declare that no funds, grants, or other support were received during the preparation of this manuscript.

## Data availability

Data sharing is not applicable to this article as no datasets were generated or analyzed during the current study.

## Declarations

**Competing interest** The authors have no relevant financial or non-financial interests to disclose.

## References

- V.A. Kulbachinskii, V. Kytin, A.A. Kudryashov, P. Tarasov, *J Solid State Chem* **193**, 47 (2012)
- Z.H. Dughaish, *Phys B Condens Matter* **322**, 205 (2002)
- S. Li, X. Zhang, Y. Lan, J. Mao, Y. Pei, Q. Zhang, Lead chalcogenide thermoelectric materials, in *Novel thermoelectric materials and device design concepts*. ed. by S. Skipidarov, M. Nikitin (Springer International Publishing, Cham, 2019), pp.83–104
- L. Chen, R. Liu, X. Shi, Review of inorganic thermoelectric materials, in *Thermoelectric materials and devices*. ed. by L. Chen, R. Liu, X. Shi (Elsevier, 2021), pp.81–145
- S. Stefanoski, M. Beekman, G. S. Nolas, in *The physics and chemistry of inorganic clathrates*. ed. by G.S. Nolas (Springer, Netherlands, Dordrecht, 2014), pp.169–191
- I.-H. Kim, *J. Korean Phys. Soc.* **72**, 1095 (2018)
- V. Zaitsev, *Ultrasonics* **43**, 21–29 (2005)
- D. Ekren, F. Azough, R. Freer, Oxide thermoelectric materials, in *Thermoelectric energy conversion*. ed. by R. Funahashi (Woodhead Publishing, 2021), pp.303–331
- J. He, Y. Liu, R. Funahashi, *J Mater Res* **26**, 1762 (2011)
- A. Page, *Half-Heusler alloys as promising thermoelectric materials* (University of Michigan Library, 2017)
- R.J. Quinn, J.W.G. Bos, *Mater Adv* **2**, 6246 (2021)
- J. Lee, S. Farhangfar, J. Lee, L. Cagnon, R. Scholz, U. Gösele, K. Nielsch, *Nanotechnology* **19**, 365701 (2008)
- S. Diliberto, V. Richoux, N. Stein, C. Boulanger, *Phys Status Solidi (a)* **205**, 2340 (2008)
- M.Y. Kim, T.S. Oh, *J Electron Mater* **38**, 1176 (2009)
- M.S. Martin-Gonzalez, A.L. Prieto, R. Gronsky, T. Sands, A.M. Stacy, *J Electrochem Soc* **149**, C546 (2002)
- M. Takahashi, M. Kojima, S. Sato, N. Ohnisi, A. Nishiwaki, K. Wakisaka, T. Miyuki, S. Ikeda, Y. Muramatsu, *J Appl Phys* **96**, 5582 (2004)
- Y. Cao, Z. Zeng, Y. Liu, X. Zhang, C. Shen, X. Wang, Z. Gan, H. Wu, Z. Hu, *J Electrochem Soc* **160**, D565 (2013)
- P. Magri, C. Boulanger, J.M. Lecuire, *Electrodeposition of Bi<sub>2</sub>Te<sub>3</sub> films* (American Institute of Physics, 1994)
- A.L. Prieto, M.S. Sander, M.S. Martín-González, R. Gronsky, T. Sands, A.M. Stacy, *J Am Chem Soc* **123**, 7160 (2001)
- V. Khairnar, A. Kulkarni, V. Lonikar, A. Gite, R. Waghmare, *Int J Sci Res Rev* **7**, 640 (2018)
- P.B. Patil, S.S. Mali, V.V. Kondalkar, R.M. Mane, P.S. Patil, C.K. Hong, P.N. Bhosale, *J Electroanal Chem* **758**, 178 (2015)
- C. Kang, H. Wang, J.H. Bahk, H. Kim, W. Kim, *Nanostruct Energy Devices* **43**, 107–141 (2015)
- G.A. Slack, D.M. Rowe, *CRC handbook of thermoelectrics* (CRC Press, 1995)
- Powder Diffract. File, JCPDS no. 15-0863, ICDD, 12 Campus Boulevard, Newtown Square, PA 19073–3273, USA, 2001
- L.D. Hicks, M.S. Dresselhaus, *Phys Rev B* **47**, 16631 (1993)
- Y. Sun, Y. Liu, R. Li, Y. Li, S. Bai, *Front Chem* (2022). <https://doi.org/10.3389/fchem.2022.865281>
- L.D. Hicks, M.S. Dresselhaus, *Phys Rev B* **47**, 12727 (1993)
- L.D. Hicks, T.C. Harman, X. Sun, M.S. Dresselhaus, *Phys Rev B* **53**, R10493 (1996)
- B. Moyzhes, V. Nemchinsky, *Appl. Phys. Lett.* **73**, 1895 (1998)

**Publisher's Note** Springer Nature remains neutral with regard to jurisdictional claims in published maps and institutional affiliations.

Springer Nature or its licensor (e.g. a society or other partner) holds exclusive rights to this article under a publishing agreement with the author(s) or other rightsholder(s); author self-archiving of the accepted manuscript version of this article is solely governed by the terms of such publishing agreement and applicable law.